AppliedChem

MDPI

Article

Catalytic Pyrolysis of Polyurethane Waste over SiO_2/Cu for Selective Production of Aniline

Thanunya Saowapark, Kanjarat Sukrat, Ukrit Amphaiphan, Chanjira Jaramornburapong, Adisak Jaturapiree and Ekrachan Chaichana *

Research Center of Natural Materials for Environment, Health and Beauty, Chemistry Program, Faculty of Science and Technology, Nakhon Pathom Rajabhat University, Nakhon Pathom 73000, Thailand; thanunya@webmail.npru.ac.th (T.S.); kanjarat@webmail.npru.ac.th (K.S.); ukrit@npru.ac.th (U.A.); chanjirajara@webmail.npru.ac.th (C.J.); adisak@webmail.npru.ac.th (A.J.)

* Correspondence: ekrachan@npru.ac.th

Abstract

This study investigated the effects of silica (SiO_2) and copper-modified silica (SiO_2/Cu) catalysts on the pyrolysis behavior and product distribution of polyurethane waste (PUW), focusing on the selective recovery of aniline, a valuable chemical intermediate. PUW pyrolysis was evaluated using thermogravimetric analysis (TGA) and a laboratory-scale batch reactor. Thermal degradation kinetics were analyzed using the Coats–Redfern method with four kinetic models: F1, A2, R3, and D3. TGA revealed two distinct degradation stages, with the F1 model providing the best fit for both stages. Both catalysts facilitated urethane hard-segment degradation during the first stage while promoting thermal stability and char formation during the second stage. Catalytic pyrolysis substantially increased aniline selectivity from 12.36 wt% for PUW to 29.66 wt% for PUW/SiO_2 and 42.38 wt% for PUW/SiO_2/Cu, attributed to the additional acidic sites introduced by Cu species. The estimated nitrogen balance showed that nitrogen recovered as aniline increased from 11.9% to 19.0% and 30.1% of the initial PUW nitrogen, respectively, while the unaccounted nitrogen fraction decreased from 64.7% to 47.2% and 38.1%. These findings suggest that SiO_2/Cu selectively directs nitrogen-containing intermediates toward recoverable aniline and may potentially reduce pathways leading to harmful nitrogenous emissions, providing a promising approach for value-added and environmentally sustainable PUW recycling.

Keywords: polyurethane waste; catalytic pyrolysis; copper-modified silica

1. Introduction

Polyurethane (PU) is one of the most widely used polymers, with an expected global growth rate of 5.6% between 2021 and 2028 [1]. It is commonly produced in foam form and is used across various industries, including construction, sports equipment, automotive, furniture, and mattresses [2]. The increasing consumption of polyurethane has consequently led to a rise in polyurethane waste (PUW). Traditional disposal methods, such as landfilling and incineration, can cause serious environmental problems. In particular, incineration of PUW under normal atmospheric conditions can release harmful gases, including hydrogen cyanide (HCN) and nitrogen oxides (NO_x), due to its high nitrogen content.

A highly promising approach for the disposal of PUW is pyrolysis, a thermal decomposition process carried out in an oxygen-free environment, which significantly reduces the formation of harmful gases. Pyrolysis is also an efficient resource-recovery method, converting waste materials into valuable products such as pyrolytic oil, syngas, and solid char.

Check for updates

Academic Editor: Raed Abu-Reziq

Received: 7 September 2026
Revised: 24 September 2026
Accepted: 26 September 2026
Published: 1 October 2026

Copyright: © 2026 by the authors. Licensee MDPI, Basel, Switzerland. This article is an open access article distributed under the terms and conditions of the Creative Commons Attribution (CC BY) license.

These products can be utilized as fuels or chemical feedstocks, supporting the principles of a circular economy [3].

Aniline and related aromatic amines are important products of PUW pyrolysis. At elevated temperatures, typically above 300 °C, urethane bond cleavage generates isocyanates, which subsequently decompose and undergo secondary reactions to form aniline and related compounds. Aniline is particularly valuable for chemical recycling because it is a key building block for producing virgin PU precursors such as methylene diphenyl diisocyanate (MDI) [4]. It is also an important platform chemical widely used in the production of dyes and pigments, rubber-processing chemicals, agrochemicals, and pharmaceuticals [5].

In the pyrolysis of PUW, the types and quality of products obtained depend on both the specific process conditions and the initial composition of the PUW. It was due to the composition of the feedstock cannot be controlled for PUW; therefore, the key factors governing the process are the operating conditions and the use of catalysts.

Silica (SiO_2) or modified silica, abundant and low-cost materials, are often used in catalytic pyrolysis of plastics such as polyethylene and polypropylene [6–8]; nevertheless, their use in polyurethane remains scarce. SiO_2 is an attractive catalyst support because of its high specific surface area, thermal and structural stability, and ability to disperse metal species effectively. In addition, surface silanol groups on SiO_2 provide weak acidic sites that can interact with polar functional groups, potentially facilitating the activation and cleavage of urethane linkages while limiting extensive secondary cracking.

The incorporation of metal species such as tin (Sn), titanium (Ti), zirconium (Zr), and copper (Cu) are common and widely studied heteroatoms chosen specifically to impart stable Lewis acidic properties to mesoporous silica, which enhance catalytic activity of catalysts [9–11]. Among the mentioned metals, Cu has benefit over others because it is drastically cheaper and more sustainable than noble metals or rarer structural metals like Zr, Hf, and Sn, making scale-up significantly more economically viable. In addition, Cu features a lower hydrogenating/cracking activity. When anchored to a silica support, it induces moderate acidity and controlled cracking, which limits over-cracking [12]. This selectively could yield valuable liquid products including aniline, rather than non-condensable gases. Highly active transition metals like nickel (Ni) and cobalt (Co) promote aggressive cracking and deep dehydrogenation, which shifts the pyrolysis product towards excessive gases and heavy char [13]. Strong metal–support interactions between Cu and SiO_2 can further improve the dispersion, stability, and accessibility of Cu species, thereby enhancing catalytic performance [14–16].

The relevance of surface acidity to polyurethane conversion is supported by recent studies showing that the cleavage of carbamate bonds over metal oxides is strongly dependent on catalyst acidity and can lead to efficient recovery of aromatic amines from polyurethane-derived compounds [17]. Moreover, Cu-based catalysts have demonstrated considerable potential for selective aromatic amine production. Cu/SiO_2 has been successfully employed for the catalytic conversion of nitrobenzene to aniline [18], while highly dispersed $Cu@SiO_2$ exhibited high chemoselectivity toward aromatic amines while suppressing undesirable side reactions [19]. More directly relevant to polyurethane recycling, a Cu-containing $ZnO–ZrO_2/Cu$ catalyst was recently shown to promote urethane-bond cleavage in a model carbamate, producing aromatic amines with high overall product yields [20]. These findings provide a mechanistic basis for selecting SiO_2/Cu in the present study, in which the weakly acidic and thermally stable SiO_2 support combined with Cu-associated active sites is expected to facilitate selective cleavage and transformation of urethane-derived intermediates toward aniline while limiting excessive secondary reactions. Although Cu-based catalysts have previously been investigated for reactions involving urethane bond cleavage and the formation of aromatic amines, their influence on the overall thermochemi-

cal conversion of PUW, including thermal decomposition behavior, product distribution, selective formation of aniline, and nitrogen migration among pyrolysis products, remains insufficiently understood.

Therefore, SiO_2/Cu catalyst is a potential candidate for PUW pyrolysis in order to tailor resulting products toward valuable chemicals especially aniline. In this study, silica was used as a catalytic support for copper modifier, prepared through a simple incipient-wetness impregnation, and also used directly as a weak acidic catalyst in the catalytic PUW pyrolysis. The pyrolysis process was carried out using two systems: thermogravimetric (TGA) pyrolysis and batch pyrolysis. The liquid products obtained from these processes were analyzed using gas chromatography–mass spectrometry (GC–MS), whereas the solid residues were characterized using a CHN analyzer. The obtained information from the TGA pyrolysis was used to construct kinetic models and then was depth-analyzed aligning with the product information to gain insights into decomposition kinetics and plausible reaction pathways. The developed process will represent a highly sustainable technology that supports chemical recycling and the circular economy. Furthermore, a comprehensive understanding of the process will establish a strong knowledge base for the further efficient utilization of polyurethane waste as a valuable resource for producing high-value chemicals.

2. Materials and Methods

2.1. Material

Polyurethane waste (PUW) was supplied by Karnyang Yeen Yong Industry Limited Partnership, Samut Prakan, Thailand. The analysis results of PUW are presented in Table 1. Silica (SiO_2), LR grade, was purchased from Chemipan Corporation Co., Ltd., Rayong, Thailand. Copper (II) nitrate trihydrate [$Cu(NO_3)_2.3H_2O$], AR grade (QRëC), was purchased from Q Chemical Co., Ltd., Bangkok, Thailand.

Table 1. Proximate and ultimate analysis of PUW.

Proximate Analysis (wt%)		Ultimate Analysis (wt%)	
Moisture content	0.13	C	65.76
Volatile matter	83.02	H	6.49
Fixed carbon	16.85	N	7.14
Ash	0	O *	20.61

* Oxygen content was calculated by difference.

2.2. Preparation of Catalyst

The catalyst was prepared by the incipient wetness impregnation method. A copper precursor solution was prepared by dissolving 0.095 g of $Cu(NO_3)_2{\cdot}3H_2O$ in 10 mL of deionized water and was subsequently added dropwise to 0.475 g of the silica support to achieve a nominal Cu loading of 5 wt%. The impregnated sample was allowed to equilibrate at room temperature for 30–60 min and then dried at 100–120 °C for 12 h. Finally, the dried material was calcined at 550 °C for 7 h in air to obtain the SiO_2/Cu catalyst. Pure silica was also employed as a catalyst in the pyrolysis experiments. It was subjected to the same drying and calcination procedures as the copper-modified silica, stored in a desiccator until use, and designated as SiO_2.

2.3. Characterization of Catalyst

2.3.1. Chemical Composition

X-ray fluorescence (XRF) spectrometer was used to determine the catalyst composition, using a PANalytical MiniPal 4 EDXRF spectrometer (PANalytical B.V., Almelo, The Netherlands), equipped with a 30 kV rhodium anode tube with a helium purge facility. A

high-resolution silicon drift detector was used to count X-rays intensity. Matrix corrections were made by using either a ratio to the Compton peak or theoretical alpha coefficients, using the minipal 4 software.

2.3.2. Morphology and Elemental Distribution

A scanning electron microscope (Mira3, TESCAN, Brno–Kohoutovice, Czech Republic) was used to examine the morphologies of the catalysts. To prevent surface charging, the samples were made conductive by coating them with a thin layer of gold using a 108 sputter coater (Cressington Scientific Instruments Ltd., Watford, UK). SEM equipped with energy-dispersive X-ray spectroscopy (EDX; EDAX unit attached to the SEM) was also employed to determine the elemental composition of the samples and to visualize the spatial distribution of elements, with accelerating voltage at 20 kV and working distance at 15 mm.

2.3.3. Acidity

The acidity of the catalysts was evaluated by ammonia (NH_3) adsorption followed by thermogravimetric analysis (TGA), based on the method described by Mara et al. [21], with slight modifications.

The catalyst was saturated with NH_3 vapor, and then purged with dry nitrogen at room temperature to removed excess gaseous and weakly physisorbed NH_3. The sample was then stored in a desiccator prior to TGA measurement. The untreated catalyst was subjected to the same drying procedure and analyzed separately as a reference.

Thermogravimetric analysis of both the untreated and NH_3-adsorbed catalysts was performed under an inert atmosphere. Approximately 10 mg of sample was heated from 40 to 600 °C at a heating rate of 1 °C min^{-1} under a nitrogen flow rate of 20 mL min^{-1}. The TGA profiles of the untreated and NH_3-adsorbed catalysts were compared to distinguish NH_3-related mass loss from background mass loss associated with adsorbed water and surface hydroxyl groups.

The amount of strongly adsorbed NH_3 was estimated from the additional mass loss of the NH_3-adsorbed catalyst relative to that of the untreated catalyst over the selected temperature range of 300–500 °C. This temperature range was selected to estimate the strongly adsorbed NH_3 fraction. NH_3 desorbed at lower temperatures may include physically adsorbed or weakly bound NH_3, whereas species retained to higher temperatures are generally associated with stronger interactions with the catalyst surface, and related to the strong acidic sites on the catalysts [22].

To minimize the influence of differences in initial moisture content and low-temperature volatile species, the mass of each sample was normalized to its value at 300 °C. The normalized mass loss between 300 and 500 °C was calculated using Equation (1):

$$\Delta W_{300-500}(\%) = \left(\frac{W_{300} - W_{500}}{W_{300}}\right) \times 100 \quad (1)$$

where W_{300} and W_{500} are the sample weights (%) recorded at 300 and 500 °C, respectively.

The NH_3-associated differential mass loss was then calculated by subtracting the normalized mass loss of the untreated catalyst from that of the corresponding NH_3-adsorbed catalyst:

$$\Delta W_{NH_3}(\%) = \Delta W_{NH_3-catalyst} - \Delta W_{catalyst} \quad (2)$$

The amount of strongly adsorbed NH_3 was subsequently calculated using Equation (3):

$$qNH_3(\mu molg^{-1}) = \frac{10,000 \times \Delta W_{NH_3}(\%)}{17.031} \quad (3)$$

where qNH_3 is the amount of strongly adsorbed NH_3 expressed as mmol NH_3 g^{-1} catalyst, ΔWNH_3 is the differential mass loss expressed as wt.%, and 17.031 g mol^{-1} is the molecular weight of NH_3. The calculated NH_3 adsorption capacity was used as an estimate of the amount of strongly adsorbed NH_3 associated with the acid sites of the catalyst.

In addition, the acid–base behavior of SiO_2 was qualitatively examined using methyl red as an indicator. SiO_2 (0.1 g) was dispersed in 10 mL of benzene followed by the addition of 3 drops of methyl red indicator solution. The suspension was mixed for 5 min at room temperature, and the resulting color was visually compared with that of a blank solution containing the same amount of methyl red without SiO_2. A color change from orange toward red indicated an acidic environment in the SiO_2 suspension.

2.3.4. Functional Groups

Fourier-transform infrared (FTIR) spectroscopy (Thermo Scientific Nicolet iS5, Thermo Fisher Scientific, Austin, TX, USA) with attenuated total reflection (ATR) was used to identify the functional groups of the catalysts. FTIR spectra were collected in transmittance mode over the range of 400–4000 cm^{-1} with a resolution of 4 cm^{-1}.

2.4. Pyrolysis of Polyurethane Waste

2.4.1. Thermogravimetric Pyrolysis

Thermogravimetric pyrolysis was performed using a Pyris 1 TGA (PerkinElmer, Inc., Shelton, CT, USA) to preliminarily investigate the thermal behavior of the samples under conditions similar to those of the actual pyrolysis. Each sample (~7 mg) was heated from 25 °C to 500 °C at a rate of 10 °C/min and then held at 500 °C for 1 h to ensure complete decomposition.

2.4.2. Kinetic Analysis

The information from TGA analysis was used for the kinetic analysis. The thermal degradation kinetics were analyzed using the Coats–Redfern integral method [23], a model-fitting approach commonly employed to determine the apparent activation energy (E_a), and the most probable reaction mechanism. Under a constant heating rate (β), the rate of solid-state decomposition is expressed as

$$\frac{d\alpha}{dt} = A\ \exp\left(-\frac{E_a}{RT}\right) f(\alpha) \tag{4}$$

where α is the conversion, t is time, A is the pre-exponential factor, E_a is the activation energy (kJ mol^{-1}), R is the universal gas constant (8.314 J mol^{-1} K^{-1}), T is the absolute temperature (K), and f(α) represents the kinetic model describing the reaction mechanism. For a constant heating rate, β = dT/dt, the Coats–Redfern approximation yields

$$\ln\left[\frac{g(\alpha)}{T^2}\right] = \ln\left(\frac{AR}{\beta E_a}\right) f(\alpha) - \frac{E_a}{RT} \tag{5}$$

where g(α) is the integral form of the reaction model. The activation energy was obtained from the slope ($-E_a/R$), while the pre-exponential factor was calculated from the intercept of the linear regression.

A series of solid-state kinetic models were evaluated, and the model providing the highest coefficient of determination (R^2) was considered to represent the dominant reaction mechanism for each decomposition stage.

F1 model (First-order reaction)

The F1 model corresponds to a first-order reaction, in which the decomposition rate is proportional to the amount of unreacted material. The differential and integral forms are

$$f(\alpha) = (1 - \alpha) \tag{6}$$

$$g(\alpha) = -\ln(1-\alpha) \tag{7}$$

The F1 model is generally associated with homogeneous chemical reactions controlled primarily by bond cleavage or molecular decomposition, where the reaction rate depends on the concentration of the remaining reactant.

A2 model (Avrami–Erofeev nucleation and growth)

The A2 model corresponds to a nucleation-and-growth mechanism described by the Avrami–Erofeev equation with an Avrami exponent of 2. The reaction proceeds through the formation of active nuclei followed by their subsequent growth. The differential and integral forms are

$$f(\alpha) = 2\Big(1 - \alpha)[-\ln(1 - \alpha)]^{1/2} \tag{8}$$

$$g(\alpha) = [-\ln(1-\alpha)]^{1/2} \tag{9}$$

The A2 model is generally associated with processes in which decomposition is controlled by the nucleation of new reaction sites and their subsequent growth. In thermal decomposition, this behavior may occur when degradation is initiated at discrete active sites within or on the surface of the solid, followed by the progressive expansion of the reacted regions.

R3 model (Three-dimensional contracting geometry)

The R3 model corresponds to a three-dimensional phase-boundary-controlled reaction, commonly described as a contracting-sphere mechanism. The reaction proceeds from the external surface toward the interior of the solid particle, resulting in a progressive decrease in the size of the unreacted core. The differential and integral forms are

$$f(\alpha) = 3\Big(1 - \alpha)^{2/3} \tag{10}$$

$$g(\alpha) = 1 - (1 - \alpha)^{1/3} \tag{11}$$

The R3 model is generally associated with heterogeneous solid-state reactions controlled by the movement of the reaction interface or phase boundary. During thermal decomposition, the reaction occurs primarily at the interface between the reacted outer layer and the unreacted inner core, with the reaction front progressively moving toward the center of the particle.

D3 model (Three-dimensional diffusion)

The D3 model corresponds to a three-dimensional diffusion-controlled mechanism described by the Jander equation. In this model, the overall decomposition rate is controlled primarily by the diffusion of reactants or volatile decomposition products through a progressively developing product or solid layer. The differential and integral forms are

$$f(\alpha) = \Big[3(1 - \alpha)^{2/3}\Big] / \Big[2\Big(1 - (1 - \alpha)^{1/3}\Big)\Big] \tag{12}$$

$$g(\alpha) = \Big[1 - (1 - \alpha)^{1/3}\Big]^2 \tag{13}$$

The D3 model is generally associated with heterogeneous solid-state reactions in which mass transport through a three-dimensional structure becomes the rate-controlling step.

During thermal decomposition, volatile products generated within the solid must diffuse through the surrounding decomposed or charred layer before being released. Consequently, the decomposition rate becomes increasingly influenced by diffusion resistance as the reaction progresses.

2.4.3. Batch Pyrolysis

Non-catalytic and catalytic pyrolysis of PUW were carried out in a 5 L stainless-steel batch reactor equipped with a nitrogen (N_2) purging system (1.5 L/min) to maintain an inert atmosphere throughout the process. For catalytic (in situ) pyrolysis, PUW and the catalysts were thoroughly mixed at a mass ratio of 4:1 before being transferred into the reactor. The reactor was then heated at a constant rate of 10 °C/min from room temperature to 500 °C, followed by an isothermal hold at 500 °C for 1 h. The reactor was then heated at a constant rate of 10 °C/min from room temperature to 500 °C, followed by an isothermal hold at 500 °C for 1 h. This temperature was selected based on a preliminary study of the PUW, which identified 500 °C as the optimum pyrolysis temperature for achieving the highest liquid yield with favorable physical characteristics. The liquid product was collected using three consecutive condensation traps immersed in ice baths and connected to the reactor gas outlet. After the reactor had cooled to room temperature, the solid product remaining in the reactor was collected and weighed. The gas yield was determined by difference from the initial feed mass after accounting for the recovered liquid and solid products. All pyrolysis experiments were performed in triplicate, and the product yields are reported as mean values ± standard deviations.

2.5. Characterization of Pyrolysis Product

2.5.1. Chemical Composition of Liquid Product

Gas chromatography–mass spectrometry (GC–MS) was used to determine the chemical composition of the pyrolytic liquids, employing a TRACE 1310 gas chromatograph (Thermo Fisher Scientific, Austin, TX, USA) equipped with a TraceGOLD™ TG-5MS capillary column (Thermo Fisher Scientific, Austin, TX, USA; 30 m × 0.25 mm i.d. × 0.25 µm film thickness). The analysis conditions were as follows: injection volume of 0.2 µL; oven temperature held at 40 °C for 1 min, then increased at 10 °C/min to 300 °C; split injection mode with a ratio of 100:1; and injector temperature of 290 °C. The chemical composition of the pyrolysis liquid was analyzed using electron ionization (EI) at 70 eV. Compounds were identified by comparison of their mass spectra with those in the NIST 20 mass spectral library. The relative content of each compound was estimated from its chromatographic peak area relative to the total integrated peak area.

2.5.2. Elemental Composition of Solid

A CHNS analyzer (Thermo Scientific™ FlashSmart™, Thermo Fisher Scientific, Milan, Italy) was used to determine the elemental composition of the samples, specifically the percentages of carbon, hydrogen, nitrogen, and sulfur. The analysis was performed following an in-house method based on ISO 16948:2015 [24].

3. Results and Discussion

3.1. Characterization of Catalyst

The prepared catalysts including SiO_2 and SiO_2/Cu were characterized using many efficient equipment. The XRF was used to determine the elemental composition of the catalysts in oxide forms based on the detected metals and metalloid, which are assumed to exist in their most stable, highest-valence stoichiometric oxide states. The major oxides compositions of the catalysts are presented in Table 2. The SiO_2 catalyst is mainly composed

of silicon oxide (silica, SiO_2) equaling to 99.02% and small amounts of CaO, TiO_2, and Fe_2O_3 totaling less than 1%. The introduction of Cu into SiO_2/Cu resulted in a Cu content corresponding to 7.24% when expressed as CuO in the normalized oxide composition. The presence of Cu significantly enhanced the apparent acidity of the SiO_2/Cu catalyst, as indicated by a strongly adsorbed NH_3 amount of 65.1 μmol NH_3 g^{-1}, whereas no strongly adsorbed NH_3 could be reliably detected for pure SiO_2. Nevertheless, the absence of detectable strongly adsorbed NH_3 does not necessarily indicate that SiO_2 is completely non-acidic, as silica can possess weakly acidic surface silanol (Si–OH) groups that may not be sufficiently strong to retain NH_3 under the applied measurement conditions. To further examine this behavior, a qualitative methyl-red indicator test was performed. The presence of SiO_2 caused the indicator color to change from orange toward red, indicating an acidic surface environment. This observation supports the presence of weak acidity on SiO_2, which may be associated with surface silanol groups. Nevertheless, more detailed characterization using NH_3-TPD and FTIR of adsorbed probe molecules, such as pyridine, would be required to quantitatively determine acid-site strength and distinguish between Brønsted and Lewis acid sites.

Table 2. Major oxides compositions of the catalysts from XRF analysis.

Sample	SiO_2	CaO	TiO_2	Fe_2O_3	CuO	Adsorbed NH_3 (μmol/g)
SiO_2	99.02	0.53	0.30	0.16	-	ND
SiO_2/Cu	91.92	0.43	0.27	0.14	7.24	65

The functional groups of the catalysts were characterized by Fourier-transform infrared (FTIR) spectroscopy, and the corresponding spectra are presented in Figure 1. Both catalysts exhibited the characteristic absorption bands of amorphous silica. Three prominent bands associated with the siloxane (Si–O–Si) framework were observed: a band at approximately 460 cm^{-1}, assigned to Si–O–Si rocking (or bending) vibrations; a band at ~800 cm^{-1}, corresponding to the symmetric stretching vibration of Si–O–Si; and a strong broad band centered at 1060–1100 cm^{-1}, attributed to the asymmetric stretching vibration of the Si–O–Si network. In addition, a weak band at approximately 950–970 cm^{-1} was assigned to the stretching vibration of surface silanol (Si–OH) groups, indicating the presence of hydroxylated surface sites. The absorption band at approximately 1630–1650 cm^{-1} was attributed to the H–O–H bending vibration of physically adsorbed water, while the broad band in the 3200–3600 cm^{-1} region corresponded to O–H stretching vibrations arising from surface silanol groups and hydrogen-bonded water molecules. These characteristic absorption bands confirm the formation of an amorphous silica framework with abundant surface hydroxyl groups [25].

Nevertheless, the silanol peak (peak 3) decreases with the introduction of Cu, as we saw that SiO_2/Cu has the mentioned peak (in dashed oval) obviously lower than that of SiO_2. This suggests that surface hydroxyl groups (−OH), as active anchoring sites for chemical adsorption, are adsorbed by copper atoms replacing the hydrogen atom and forming Cu−O−Si bonds. Thus, the free silanol groups are consumed, leading to the drop in silanol peak. This drop confirms the formation of Cu with SiO_2 surface through chemical linkages, and then change surface nature of the catalysts.

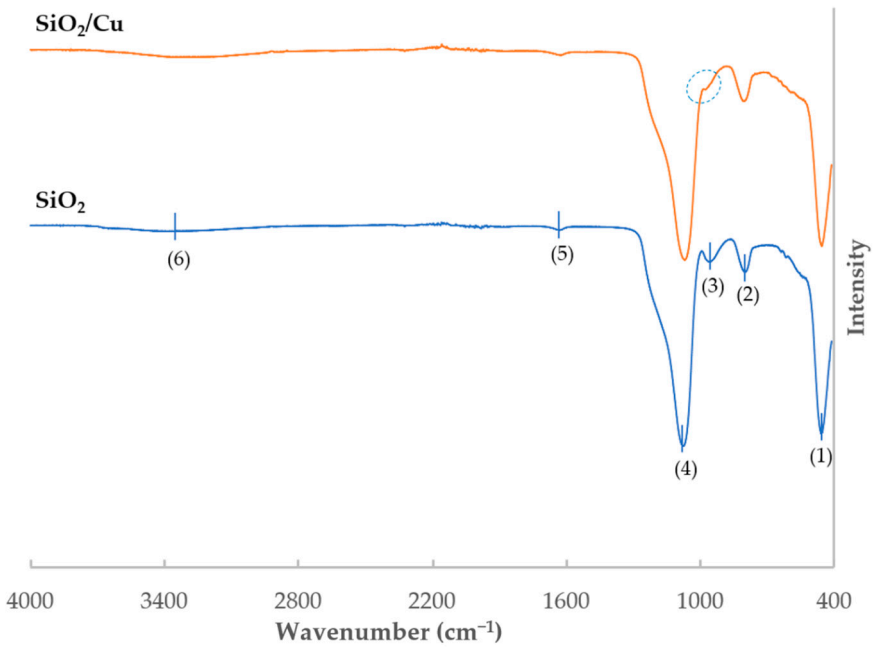


Figure 1. FTIR spectra of SiO_2 and SiO_2/Cu: (1) Si-O-Si bond rocking, (2) symmetric Si–O–Si stretching, (3) surface Si–OH stretching, (4) Asymmetric Si–O–Si stretching, (5) H–O–H bending of adsorbed water, and (6) O–H stretching of silanol groups and hydrogen-bonded water.

Morphologies of the catalysts were analyzed using an SEM measurement, and the SEM images of the catalysts with two magnifications are presented in Figure 2. Both catalysts exhibit the same particle appearance with a rounded to sub-angular morphology and relatively smooth surfaces. The particles of SiO_2/Cu appear well separated without noticeable agglomeration, indicating that the silica support maintains its original morphology, suggesting that the impregnation process does not significantly alter the macroscopic structure of the silica support. No severe particle sintering or structural collapse is observed after Cu loading.

At higher magnification, the SiO_2 surface appears relatively smooth and homogeneous with only a few fine surface asperities. After Cu impregnation, numerous bright particles are observed on the silica surface. From an SEM/EDX mapping of SiO_2/Cu (on Si, Cu, and O elements), as illustrated in Figure 3, it indicates that those particles are a cluster of Cu species. Nevertheless, the Cu signal is also detected across much of the surface outside these clusters, suggesting that a considerable fraction of Cu remains finely dispersed on the silica support. The high dispersion of Cu species likely contributed to the enhanced Lewis acidity of the catalyst [26], as suggested by the presence of additional strongly adsorbed NH_3 species.

The Si elemental map exhibits localized regions of reduced intensity that spatially correspond to Cu-rich areas observed in the Cu map. This decrease in Si signal is attributed to the deposition of Cu species on the silica surface, which partially attenuates the Si X-rays detected by EDX. In contrast, the O elemental map remains relatively homogeneous. This observation suggests that oxygen is present in both the silica support (SiO_2) and the deposited Cu species, which indicates that the Cu species observed exist as the oxide forms. This result is in consistent of the FTIR spectrum and the assumption of XRF analysis.

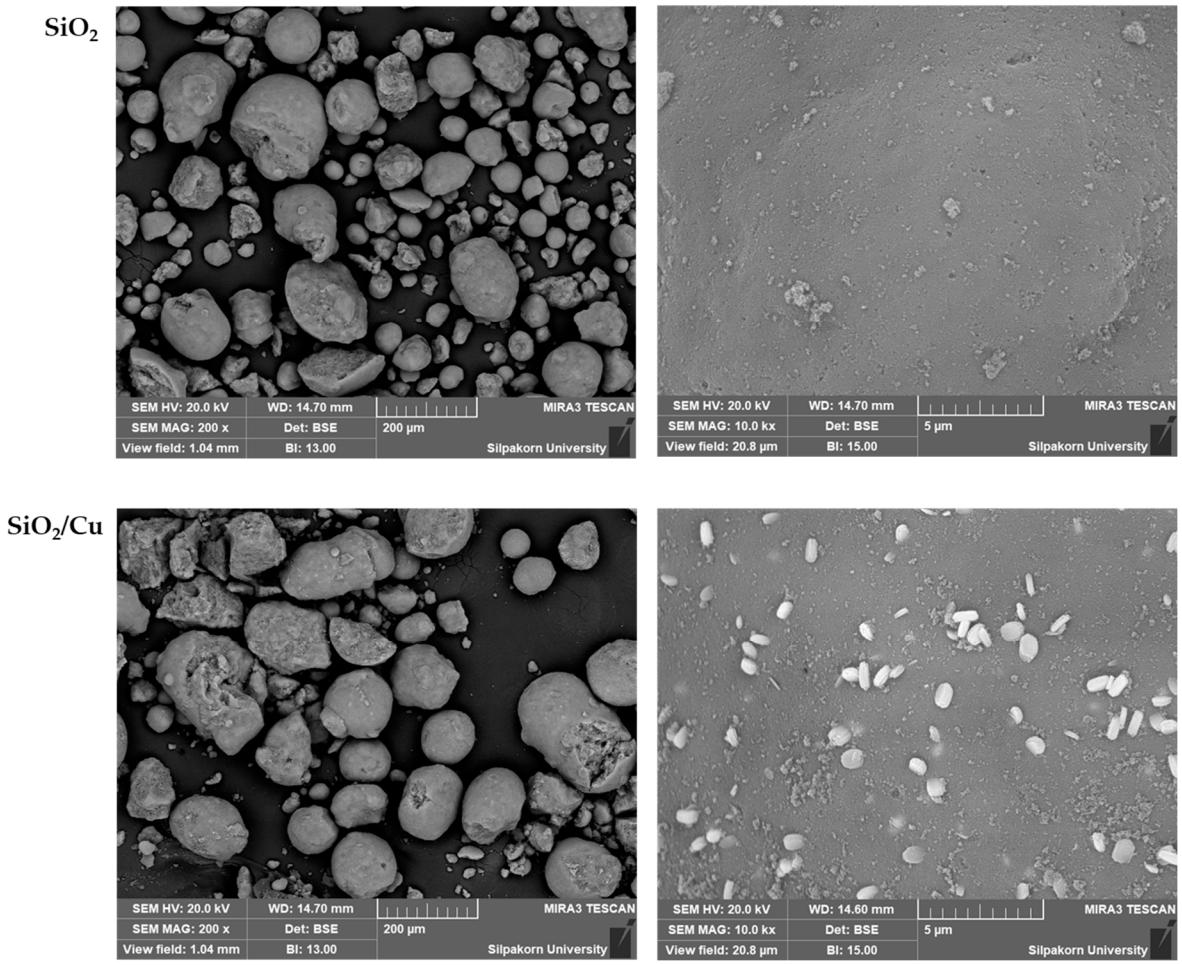


Figure 2. SEM images of the catalysts with two magnifications.

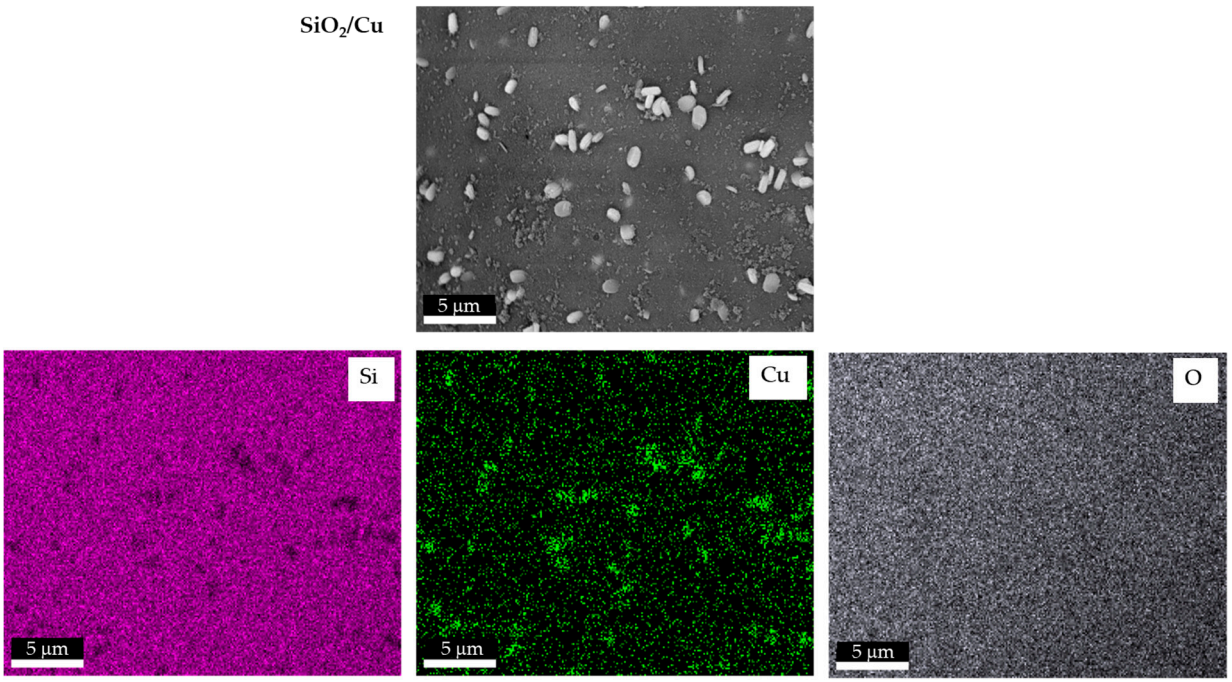


Figure 3. EDX mapping of SiO_2/Cu for Si, Cu, and O elements.

3.2. Pyrolysis of PUW

Micro-scale catalytic pyrolysis of pure polyurethane waste (PUW), polyurethane waste in the presence of catalysts namely SiO_2 (PUW_SiO_2) and SiO_2/Cu (PUW_SiO_2/Cu) were conducted using TGA equipment. The pyrolysis conditions were adjusted similarly to the further batch pyrolysis, including the ratio of feedstock to catalyst (4:1), heating rate of 10 °C/min, reaction temperature of 500 °C, and holding for 1 h under N_2 atmosphere. The TGA curves (mass change against temperature) and DTG curves (rate of mass change against temperature), which replicate the pyrolysis phenomena of all samples, are represented in Figures 4 and 5.

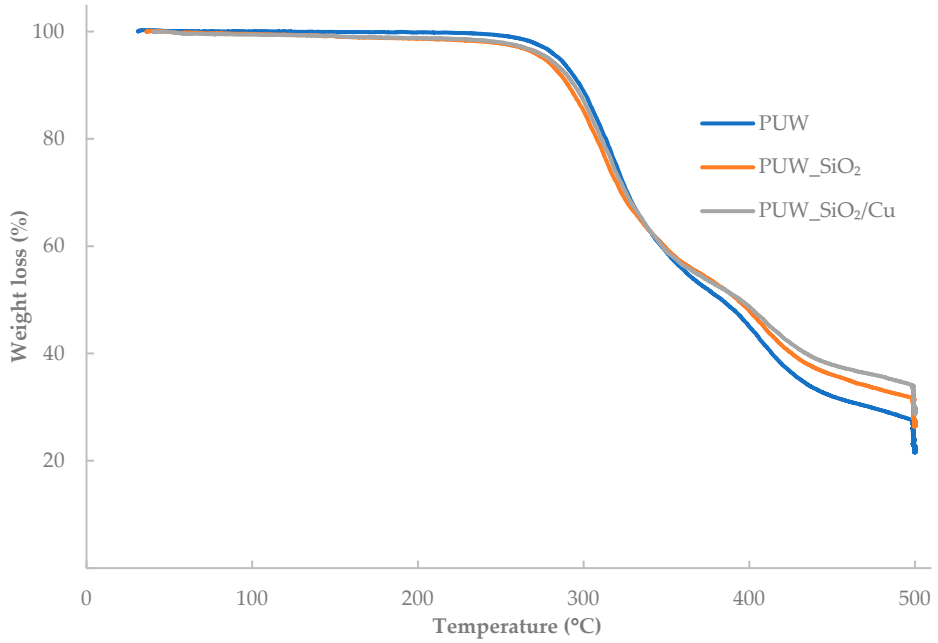


Figure 4. TGA curves of PUW and PUW mixed with catalysts.

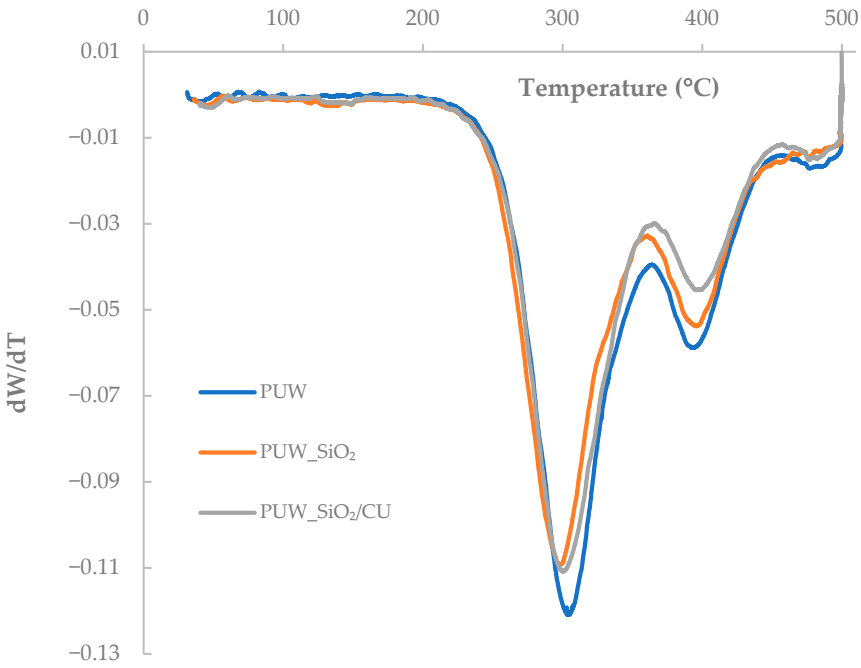


Figure 5. DTG curves of PUW and PUW mixed with catalysts.

As the pyrolysis process included an isothermal holding period at 500 °C to complete the reaction, the TGA and DTG curves were plotted as a function of time, with temperature included on a secondary *Y*-axis (Figure 6), to distinguish the thermal behavior during dynamic heating from that during the isothermal period. For clarity, only the curves for PUW are presented, as the other samples exhibited similar patterns. The DTG profiles plotted as a function of time exhibit peaks at approximately 300 °C, indicating that the principal decomposition event occurred during the heating stage. Additional decomposition was observed at higher temperatures, consistent with the multistep degradation behavior of PUW. After the temperature reached 500 °C, the DTG signal approached zero for all samples, indicating a substantial decrease in the decomposition rate during the isothermal period. Nevertheless, the corresponding TGA curves showed a gradual additional mass loss during this period, suggesting that slow decomposition and/or secondary reactions continued at 500 °C. Thus, plotting the thermal data against time clearly distinguishes the rapid decomposition occurring during dynamic heating from the slower mass-loss processes during the subsequent isothermal stage.

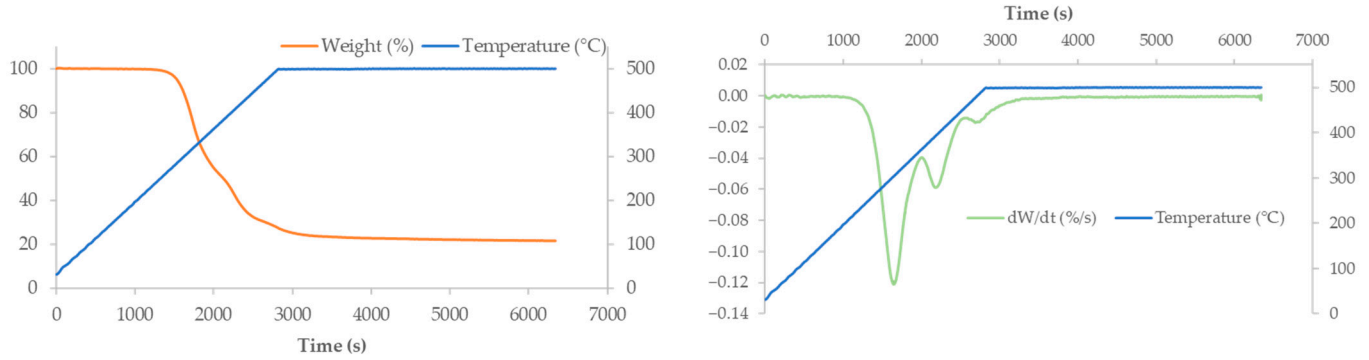
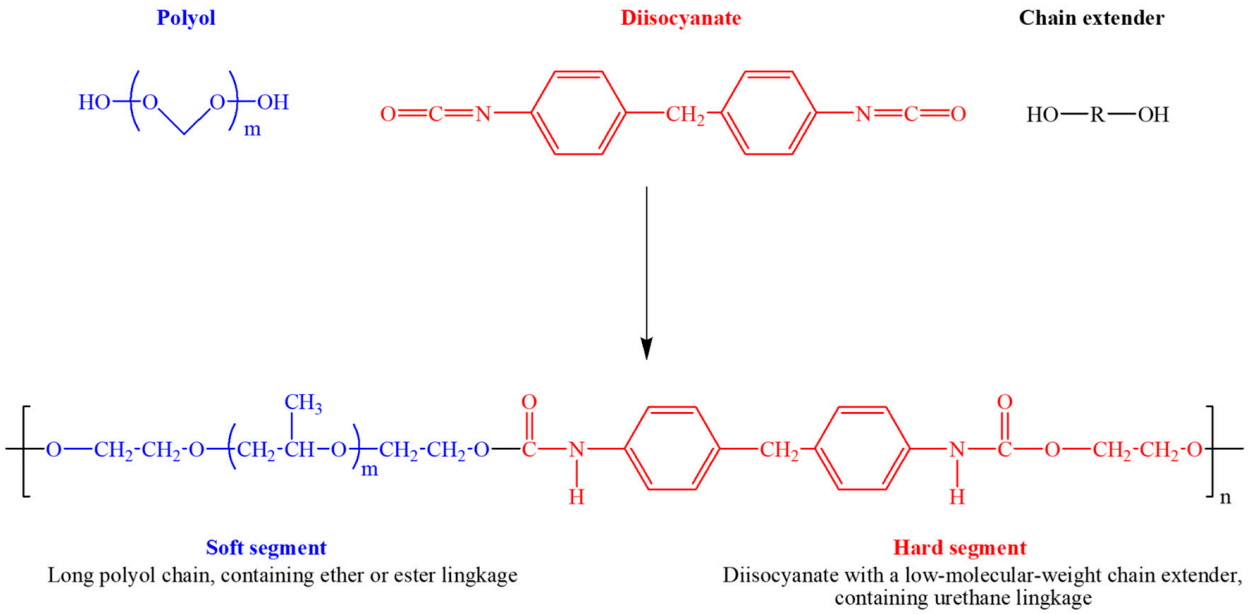


Figure 6. TGA and DTG plotted as a function of time for PUW.

For the first DTG plot (Figure 5), all samples exhibit two distinct thermal degradation stages, the first stage approximately 245–350 °C with maximum temperature (T_{max1}) about 300 °C and the second range of 365–430 °C with maximum temperature (T_{max2}) about 395 °C. Polyurethanes are segmented block copolymers consisting of alternating hard and soft segments (Scheme 1). Owing to their microphase-separated structure and the different thermal stabilities of these two domains, polyurethane materials typically undergo thermal degradation in two consecutive stages during a TGA scan [27]. The first stage represents the dissociation and cleavage of the urethane bonds (−NH−CO−O−) in the hard segments into primary amines, alcohols, and carbon dioxide. In the second, the degradation involves the cracking and volatilization of the polyol soft segments (polyesters or polyethers).

Based on the TGA and DTG results, the Coats–Redfern method was applied to evaluate the thermal degradation kinetics using four solid-state kinetic models representing different possible rate-controlling mechanisms: F1 (first-order reaction), A2 (two-dimensional nucleation and growth), R3 (three-dimensional phase-boundary contraction), and D3 (three-dimensional diffusion). These models were selected to provide a comparative assessment of reaction-controlled, nucleation-controlled, phase-boundary-controlled, and diffusion-controlled descriptions of PUW decomposition. The kinetic parameters obtained by the Coats–Redfern method are model- and analysis-dependent and may vary with the selected temperature and conversion ranges, stage definition, kinetic model, and data-processing procedure. Consequently, the calculated E_a and A values are most appropriately used for comparative evaluation of PUW, PUW/SiO_2, and PUW/SiO_2/Cu analyzed under identical conditions. The obtained values including apparent activation energy (E_a), pre-

exponential factor (A), and coefficient of determination (R^2) for each degradation stage are summarized in Table 3.



Scheme 1. Polyurethane formation from polyol, diisocyanate, and chain extender, showing the soft and hard segment structures.

Table 3. Maximum temperatures (T_{max}), estimated activation energies (E_a), pre-exponential factor (A), and the coefficient of determination (R^2) for the thermal decomposition of PUW and PUW mixed with catalysts.

Sample	1st-Stage Decomposition					2nd-Stage Decomposition				
	T_{max1} (°C)	Model	E_a (kJ/mol)	A (min^{-1})	R^2	T_{max2} (°C)	Model	E_a (kJ/mol)	A (min^{-1})	R^2
PUW	303.1	F1	150.14	7.63×10^{12}	0.9973	394.3	F1	218.61	3.43×10^{16}	0.9895
		A2	70.24	3.47×10^{5}	0.9968		A2	103.74	2.47×10^{7}	0.9883
		R3	134.56	2.39×10^{11}	0.9893		R3	194.5	3.53×10^{14}	0.9794
		D3	278.78	2.03×10^{23}	0.9902		D3	400.14	4.04×10^{29}	0.9806
PUW_SiO_2	300.1	F1	140.73	1.26×10^{12}	0.9907	396.7	F1	222.99	7.25×10^{16}	0.9895
		A2	65.55	1.37×10^{5}	0.9891		A2	105.92	3.63×10^{7}	0.9882
		R3	125.41	4.07×10^{10}	0.9778		R3	198.47	6.96×10^{14}	0.9795
		D3	260.45	6.29×10^{21}	0.9796		D3	408.1	1.55×10^{30}	0.9806
PUW_SiO_2/Cu	301.8	F1	144.34	2.35×10^{12}	0.9955	398.6	F1	209.78	6.55×10^{15}	0.9865
		A2	67.34	1.89×10^{5}	0.9947		A2	99.32	1.06×10^{7}	0.9849
		R3	129.44	8.45×10^{10}	0.9863		R3	186.96	8.55×10^{13}	0.9774
		D3	268.53	2.63×10^{22}	0.9874		D3	385.06	2.47×10^{28}	0.9787

Among the four models examined, F1 exhibited the highest R^2 values for all samples in both degradation stages, indicating that the overall degradation kinetics can be most satisfactorily described by an apparent first-order reaction model. It assumes chemical reactions controlled primarily by bond cleavage or molecular decomposition, where the reaction rate depends on the concentration of the remaining reactant. Nevertheless, because polyurethane degradation involves several simultaneous and consecutive reactions, assignment of the F1 model should be regarded as an apparent kinetic description rather than evidence of a single elementary first-order reaction.

During the first stage, PUW has lower weight loss and higher T_{max1} than those of PUW_SiO_2 and PUW_SiO_2/Cu. These results indicate that the presence of the catalysts reduces thermal stability of polyurethane, suggesting that the silica-based catalysts enhance structural destabilization of polyurethane. In addition, the F1 activation energy decreased from 150.14 kJ mol^{-1} for PUW to 140.73 and 144.34 kJ mol^{-1} for PUW/SiO_2 and PUW/SiO_2/Cu, respectively, partially supporting that the catalysts facilitate the initial degradation reactions. Nevertheless, only slightly lower values may not be considered conclusive evidence of a catalytic effect on the activation energy. The realiable explanation should be associated with plausible phenomena occuring during the process. As found from that SiO_2 also possesses apparent acidity, its weakly acidic sites (silanol group, Si–OH) may interact with urethane functionalities during thermal decomposition, and facilitate the thermal cleavage of urethane linkages, thereby lowering the activation energy required for the initial dissociation of urethane bonds [25].

For SiO_2/Cu, it influences the first stage degradation of polyurethane similarly to SiO_2 due to having main composition of silica. Nevertheless, the addition of measurable strongly adsorbed NH_3 sites (plausible Lewis acidic sites) of SiO_2/Cu could provide stronger interactions between Cu-associated Lewis acid sites and the carbonyl oxygen of urethane groups. Although these interactions can promote activation of the urethane linkage, stronger coordination may also stabilize adsorbed urethane species or reaction intermediates [17], resulting in a slightly higher apparent energy barrier for the initial decomposition step, and thus the slightly higher E_a of PUW/SiO_2–Cu compared with PUW/SiO_2.

In the second stage of decomposition, both SiO_2 and SiO_2/Cu reverse roles to provide better thermal stability to the polymer, as observed that the TGA curves of the catalytic pyrolysis cross above the pure PU and have slower downward slopes [28]. As the physical barriers, the catalyst crusts slow down heat transfer into the remaining soft segments and drastically lowering their rate of mass loss compared to pure, unprotected PU, which is in consistent with the DTG curves [29]. In addition, the higher F1 activation energies in Stage II than in Stage I indicate that decomposition of the material remaining after primary urethane cleavage requires a larger apparent energy barrier, which involves the breakdown of rigid isocyanate moieties and char formation [30]. PUW/SiO_2 shows a slightly higher Stage II (E_a) (222.99 kJ mol^{-1}) than neat PUW (218.61 kJ mol^{-1}), which is consistent with a modest stabilization of the residual structures. In contrast, PUW_SiO_2/Cu exhibited the lowest Stage II activation energy (E_a) of 209.78 kJ mol^{-1}, suggesting dual effects of the catalyst. The silica network of SiO_2/Cu acts as a physical mass and thermal barrier that shifts the second-stage decomposition onset to a higher temperature window. However, once decomposition initiates, the active Cu sites catalyze the chemical cracking of polyol segments. This transitions the degradation into an energetically favorable pathway, reducing the overall activation energy (involving multiple competing reactions) compared to the pristine PU control.

Batch pyrolysis of all samples was further conducted using a 5 L stainless steel reactor equipped with a nitrogen (N_2) gas purging system, with heating rate of 10 °C/min, ramping from room temperature to 500 °C, followed by isothermal holding at 500 °C for 1 h. The product yields of the pyrolysis are presented in Figure 7. The pristine PUW produced the highest liquid yield (45.9 wt%), whereas the use of SiO_2 decreased the liquid yield to 30.4 wt% and increased the gas yield to 51.7 wt%, indicating enhanced cracking of pyrolysis vapors. Incorporation of Cu into the SiO_2 catalyst partially recovered the liquid yield to 33.7 wt% while reducing the gas yield to 45.6 wt%, suggesting that Cu modified the catalytic reaction pathway by promoting the formation of condensable products and suppressing some secondary reactions, which turn condensable intermediates into gaseous products.

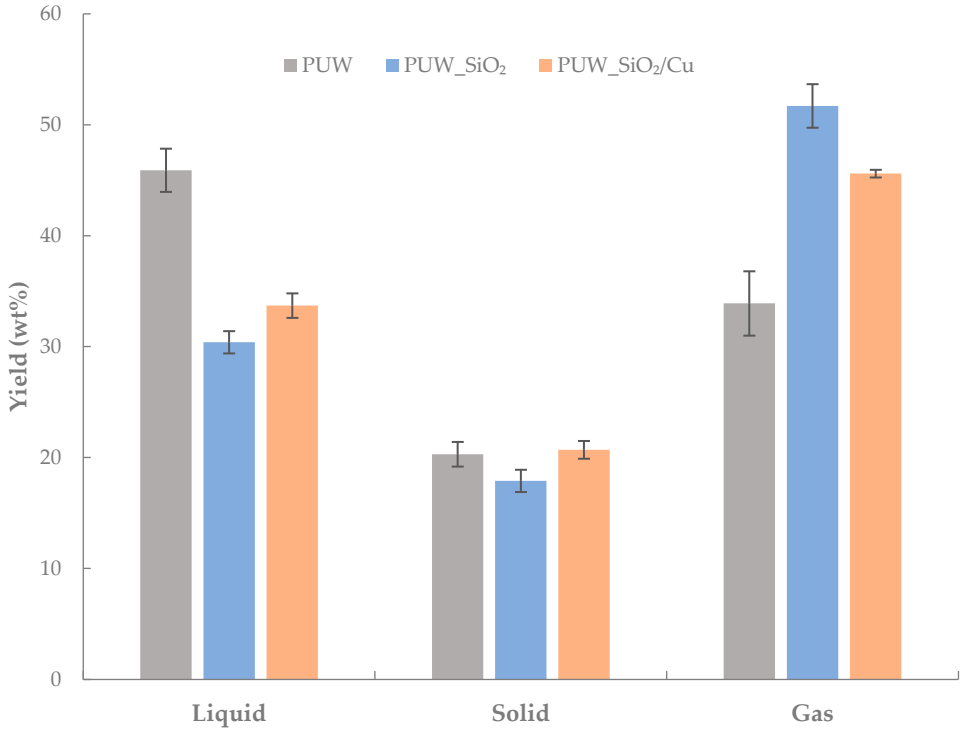


Figure 7. Product yields from the pyrolysis of various samples, with standard deviation error bars.

It can be noticed that the product distribution agrees well with the TGA results or the micro-scale pyrolysis. The reduced thermal stability observed during the first degradation stage indicates that both SiO_2 and SiO_2/Cu promoted the initial cracking of PUW, generating a greater amount of volatile compounds and consequently increasing the gas yield, and decreasing the liquid yield. Conversely, the higher thermal stability in the second degradation stage suggests that the catalysts altered the decomposition pathway, leading to the formation of more thermally resistant intermediates or carbonaceous residues (solid yield). Previous studies have also shown that nanosilica used as a filler in polyurethane composites enhances their thermal stability and promotes char formation [31].

3.3. Characterization of Pyrolysis Products

Chemical composition of the pyrolysis products including condensable liquids and solids were characterized using GC-MS and CHNS analyzer, respectively. The compositional profiles of the product provide insights into the reaction mechanisms and transformation pathways occurring during pyrolysis, in the absence and presence of catalysts. Table 4 presents the compound groups of the liquid products analyzed from GC-MS, which were classified into eight groups, and also the amount of specific compounds, namely aniline at the bottom of the table.

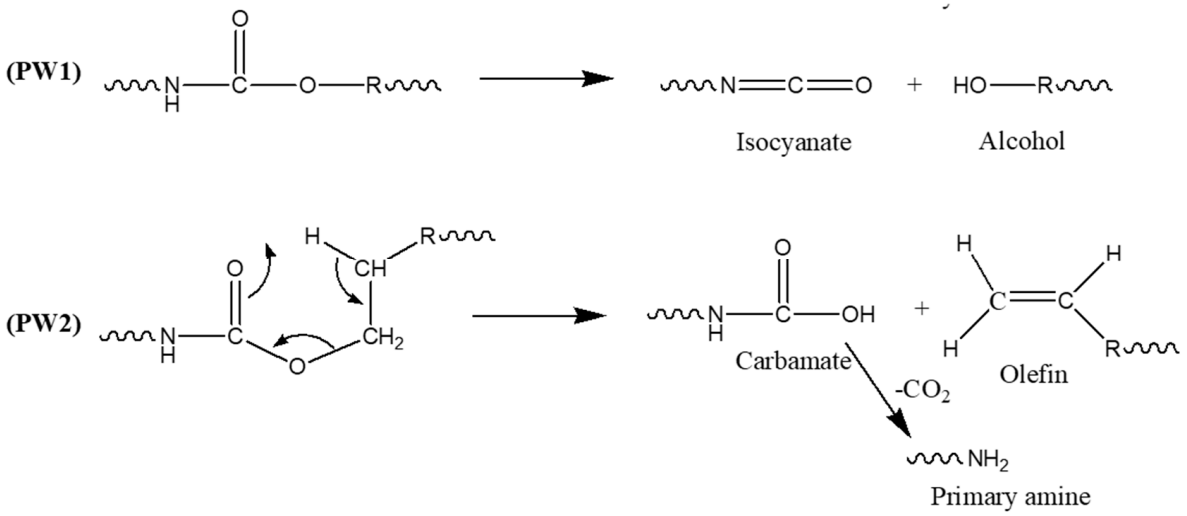
The GC–MS analysis revealed that the catalysts markedly altered the composition of the pyrolysis oil. Pyrolysis of pure PUW produced bio-oil was dominated by aromatic hydrocarbons (56.9 wt%), whereas catalytic pyrolysis substantially reduced their proportion to 24.5 wt% over SiO_2 and 21.6 wt% over SiO_2/Cu. Conversely, aromatic amines increased significantly from 14.1 wt% for pure PUW to 29.7 wt% and 42.4 wt% in the presence of SiO_2 and SiO_2/Cu, respectively, with aniline being the predominant compound. The liquid composition results further demonstrate that the catalysts substantially promoted the selective recovery of aniline (yield based on PUW feedstock), despite the changes in overall liquid yield shown in Figure 7. These results indicate that the catalytic effect, particularly

that of SiO_2/Cu, favors selective recovery of nitrogen as the value-added product aniline rather than maximizing the overall liquid yield.

Table 4. Classification and relative contents of compounds identified in the pyrolytic liquids from various samples by GC–MS.

Compound	PUW	PUW_SiO_2 (wt%)	PUW_SiO_2/Cu
Aromatic hydrocarbons	56.9	24.5	21.6
Aromatic amines	14.1	29.7	42.4
Oxygenated heterocycles	11.4	5.9	8.9
Ethers/glycol ethers	7.0	14.2	7.8
Aliphatic hydrocarbon	3.4	11.7	10.5
Ketones	2.1	6.1	4.6
Alcohols	1.8	4.5	2.5
Others	3.3	3.4	1.7
Aniline			
Yield in liquid	12.4	29.7	42.4
Yield based on PUW feedstock	5.7	9.0	14.3

From the TGA analysis, it suggests that the catalysts altered the decomposition pathway of PUW. Consequently, the shift toward more selective reaction pathways in the presence of the catalysts likely accounts for the increased formation of specific products, particularly aniline. The primary thermal decomposition pathways of a typical polyurethane have been previously proposed by Hiltz [32], as illustrated in Scheme 2. It suggests that the decomposition of PU proceeds through two primary mechanisms: PW1: dissociation of the urethane linkage to yield an isocyanate and an alcohol as products; and PW2: a rearrangement via a six-membered transition state that produces a primary amine, an olefin, and carbon dioxide (CO_2).



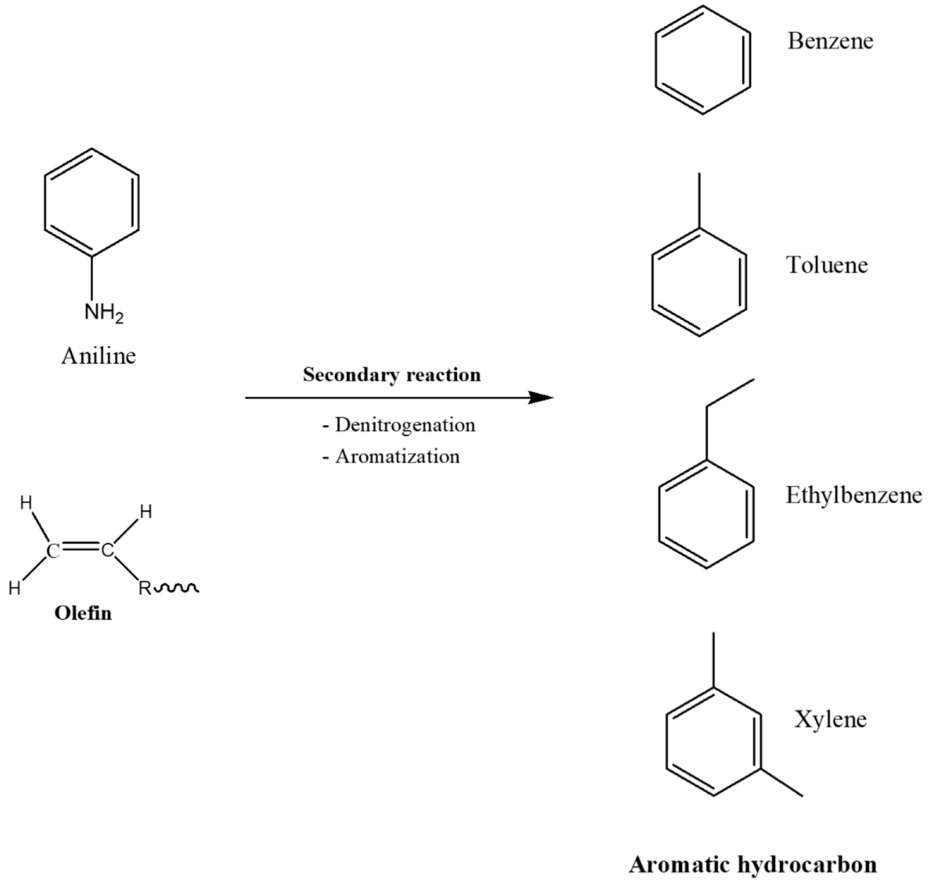
Scheme 2. Proposed primary thermal decomposition pathways of typical polyurethane.

Based on the GC-MS results, it suggests that the catalysts shift the first-stage decomposition toward PW2. It is indirectly evident by the strong increase in primary aromatic amines and aliphatic hydrocarbons, and the substantial decrease in aromatic hydrocarbon, which is diverted away toward amine formation. The catalysts can promote PW2 due to possessing numerous Lewis acidic Si sites and surface silanol (Si–OH) groups. The acidic sites polarize the urethane carbonyl (C=O), weaken the C–O bond, stabilize the cyclic

transition state proposed for PW2, and facilitate decarboxylation of carbamate [33]. As a result, carbamate intermediates form more readily, carbamates decompose more readily, and primary amines (aniline) are produced in higher amounts. The addition Cu species on the catalyst (SiO_2/Cu) can activate more C–N and C–O bonds, facilitate hydrogen transfer, and stabilize aromatic amine intermediates. Therefore, a higher aniline production than that of SiO_2 occurs.

In addition, during PUW pyrolysis at 500 °C, reducing gases and intermediates, particularly CO and H_2, may promote the partial reduction of CuO through Cu(II) → Cu(I) and potentially Cu(0) [34]. This reaction may provide additional pathways for electron transfer and interactions with oxygen- and nitrogen-containing intermediates. Such dynamically evolving Cu species may therefore contribute to the altered decomposition pathways and enhanced formation of aniline observed over SiO_2/Cu. Nevertheless, because the oxidation state of Cu was not characterized under reaction conditions, the specific contribution of Cu^{2+}, Cu^{+}, and Cu^{0} species cannot be conclusively distinguished in the present study.

The catalysts also likely suppressed secondary reactions, including denitrogenation and aromatization, which convert aromatic amines and olefins into aromatic hydrocarbons, as presented in Scheme 3. This is consistent with the reduced yield of aromatic hydrocarbons observed in the products obtained from catalytic pyrolysis over both SiO_2 and, more prominently, SiO_2/Cu.



Scheme 3. Proposed secondary reaction pathways for the formation of aromatic hydrocarbons from aniline and olefin intermediates during polyurethane pyrolysis.

The denitrogentaion (removal of nitrogen or nitrogen-containig compound) occurs at temperatures between 500 °C and 600 °C, typically with strong acid catalysts like HZSM-5 [35]. High heat breaks weak carbon-nitrogen bonds, releasing nitrogen fragments as ammonia (NH_3) or hydrogen cyanide traces, while strong acidic sites actively pull off the

amino group. As observed in the TGA analysis, the silica-based catalysts enhanced the thermal stability of PUW, thereby reducing the breaking of carbon–nitrogen bonds and retaining nitrogen-containing fragments longer in the condensed phase, which slow down the toxic "smoke" kinetics (generating of harmful nitrogen emission) and crack down into less volatile amine complexes [36]. For SiO_2/Cu, dispersed Cu species are proposed to modify the reaction pathway by promoting selective hydrogen transfer, thereby favoring the preservation of aromatic amines [37]. In addition, the lone pair of electrons on the nitrogen atom of the amino group can readily coordinate with surface Cu sites. This Lewis acid–base interaction may stabilize aniline on the catalyst surface, reducing its susceptibility to further thermal decomposition and secondary reactions, such as deamination and aromatization, into aromatic hydrocarbons.

Aromatization is promoted by the formation of highly reactive olefinic intermediates generated during the first-stage decomposition, together with volatile radical fragments released from the polyol chains during the second-stage decomposition. These intermediates undergo cyclization, hydrogen transfer, and dehydrogenation reactions, leading to the formation of aromatic hydrocarbons. The silica support may also act as a physical barrier during the second decomposition stage, isolating reactive intermediates and hindering their condensation into larger aromatic structures [38]. Furthermore, the incorporation of Cu is likely to modify the reaction pathway by promoting hydrogen-transfer reactions and stabilizing reactive olefinic intermediates, thereby suppressing their cyclization and subsequent aromatization into aromatic hydrocarbons.

It should be noted that PUW/SiO_2–Cu exhibited the lowest apparent activation energy during the second decomposition stage. This indicates that the activation energy derived from TGA represents the apparent energy barrier associated with the overall mass-loss process and does not directly describe the activation barriers of individual secondary reactions. PU decomposition involves multiple parallel and consecutive reactions, including urethane-bond cleavage, decomposition of isocyanate-derived intermediates to aromatic amines, and subsequent reactions of these products. Therefore, the lower apparent E_a of PUW/SiO_2–Cu may indicate that Cu-containing active sites facilitate the decomposition of thermally stable PU-derived intermediates and promote pathways leading to aniline formation. Meanwhile, SiO_2/Cu may suppress further conversion of the initially formed aromatic amines through competing secondary reactions, including nitrogen-loss and aromatic-product-forming pathways, thereby preserving a larger fraction of aniline in the liquid product. Accordingly, the lower apparent activation energy during Stage II and the enhanced aniline yield can be considered complementary effects of SiO_2/Cu on reaction kinetics and product selectivity.

The elemental compositions of the chars produced from all pyrolysis experiments were determined using a CHN analyzer, with the results summarized in Table 5.

Table 5. Elemental compositions and H/C and N/C ratios of chars produced from the pyrolysis of PUW and PUW mixed with catalysts.

Sample	C	H	N	O *
		(wt%)		
PUW	66.62	4.49	7.50	21.39
PUW_SiO_2	45.88	2.48	5.60	46.04
PUW_SiO_2/Cu	33.89	2.75	4.80	58.56

* Oxygen content was calculated by difference.

The carbon, hydrogen, and nitrogen contents decreased in the recovered solids obtained from catalytic pyrolysis. This decrease can be attributed to the presence of residual SiO_2-based catalysts, which are not directly quantified by CHN elemental analysis and

therefore dilute the measured C, H, and N contents, resulting in lower apparent concentrations in the catalyst-containing solids. Nevertheless, these data can be used to estimate the distribution of nitrogen among the pyrolysis products, providing additional evidence to support the degradation pathways proposed earlier. Based on the ultimate analysis of PUW, pyrolysis product yields, GC–MS analysis of the liquid products, and CHN analysis of the recovered solids, the nitrogen balance during pyrolysis, including the fraction of nitrogen recovered as aniline, was estimated, as presented in Table 6.

Table 6. Nitrogen balance during pyrolysis of PUW and PUW mixed with catalysts.

Sample	N in Liquid	N in Solid (wt%)	N in Gas *	N as Aniline (wt%)
PUW	14.0	21.3	64.7	*11.9*
PUW_SiO_2	19.2	33.6	47.2	*19.0*
PUW_SiO_2/Cu	31.2	30.7	38.1	*30.1*

* N in gas was estimated as unaccounted nitrogen, calculated by subtracting the nitrogen quantified in the liquid and solid products by GC–MS and CHN analysis, respectively, from the total nitrogen in the feedstock.

The estimated fraction of initial PUW nitrogen retained in the recovered solid increased from 21.3% for non-catalytic PUW to 33.6% and 30.7% for PUW_SiO_2 and PUW_SiO_2/Cu, respectively. More importantly, the estimated nitrogen recovered in the liquid fraction increased from 14.0% for PUW to 19.2% for PUW_SiO_2 and 31.2% for PUW_SiO_2/Cu. Approximately 30.1% of the initial PUW nitrogen was recovered specifically as aniline in the SiO_2/Cu-catalyzed system, compared with 11.9% for non-catalytic pyrolysis. Consequently, the nitrogen fraction decreased in the gas fraction (unaccounted nitrogen) from approximately 64.7% for PUW to 47.2% for PUW_SiO_2 and 38.1% for PUW_SiO_2/Cu. These results are consistent with SiO_2/Cu directing nitrogen-containing intermediates toward condensed products, particularly aniline, while reducing pathways associated with nitrogen loss include denitrogenation and deamination.

From an environmental perspective, the redistribution of nitrogen toward condensed products may provide an additional benefit of catalytic PUW pyrolysis by probably reducing the release of nitrogen-contained toxic gases such as NH_3 and HCN. However, because gaseous nitrogen species were not directly quantified in the present study, the decrease in unaccounted nitrogen cannot be directly attributed to reduced NH_3, HCN, N_2, or NO_x formation. Previous studies on the thermal conversion of waste rigid polyurethane foam have demonstrated that the oxide catalysts (Ca, Mg, and Mn) did not only alter the nitrogen migration among the products, but also specifically influence the gaseous product compositions including nitrogen-containing species [39]. Therefore, further quantitative analysis of the gaseous products is required to confirm the proposed nitrogen-migration behavior and its potential environmental benefits.

4. Conclusions

This study investigated the effects of silica (SiO_2) and copper-modified silica (SiO_2/Cu) catalysts on the pyrolysis of polyurethane waste (PUW). Both catalysts accelerated the degradation of urethane hard segments during the first stage while enhancing thermal stability in the second stage, with the F1 model providing the best fit for the decomposition kinetics in both stages. Copper modification increased the apparent acidity of the catalyst through the introduction of additional Lewis acid sites, contributing to its enhanced catalytic performance. Product analysis demonstrated that both catalysts promoted the selective formation of aniline, with SiO_2/Cu exhibiting superior performance to pristine SiO_2. The estimated nitrogen balance further revealed that SiO_2/Cu effectively directs nitrogen-

containing intermediates toward the formation of recoverable aniline while potentially limiting pathways associated with the release of undesirable gaseous nitrogen species.

Author Contributions: Methodology, T.S., A.J. and E.C.; investigation, T.S., K.S., U.A., C.J. and A.J.; validation, formal analysis, T.S. and E.C.; funding acquisition, T.S.; project administration, A.J. and E.C.; conceptualization, writing—original draft preparation, writing—review and editing, E.C. All authors have read and agreed to the published version of the manuscript.

Funding: This research was funded by Thailand Science Research and Innovation (TSRI), grant number TSRI_68_2.1.

Institutional Review Board Statement: Not applicable.

Informed Consent Statement: Not applicable.

Data Availability Statement: Data will be made available as requested.

Acknowledgments: The authors would like to thank the Center of Excellence in Glass Technology and Materials Science (CEGM) and the Scientific and Technological Equipment Centre (STEC) for providing facilities and analysis support.

Conflicts of Interest: The authors declare no conflicts of interest.

References

1. Donadini, R.; Boaretti, C.; Lorenzetti, A.; Roso, M.; Penzo, D.; Dal Lago, E.; Modesti, M. Chemical Recycling of Polyurethane Waste via a Microwave-Assisted Glycolysis Process. *ACS Omega* **2023**, *8*, 4655–4666. [CrossRef] [PubMed]
2. Font, R.; Fullana, A.; Caballero, J.A.; Candela, J.; García, A. Pyrolysis study of polyurethane. *J. Anal. Appl. Pyrolysis* **2001**, *58–59*, 63–77. [CrossRef]
3. Thiagarajan, C.; Yuvarajan, D.; Channappagoudra, M.; Bhanot, D.; Upadhye, V.J.; Choudhury, S.; Shukla, K.K. Advancing sustainable medical waste management: The role of pyrolysis in resource recovery and environmental protection. *Results Chem.* **2025**, *17*, 102639. [CrossRef]
4. Zeller, M.; Wattenberg, L.; Shrestha, P.; Hannemann, A.; Erdenepurev, A.-E.; Netsch, N.; Bergfeldt, B.; Tavakkol, S.; Stapf, D. Characteristics of Polyurethane Pyrolysis—Experimental Investigations and Product Analyses for the Assessment of Chemical Recycling Potentials. *J. Appl. Polym. Sci.* **2026**, *143*, e70032. [CrossRef]
5. Mary, A.; Kanagathara, N.; Baby Suganthi, A.R. A brief review on aniline and its derivatives. *Mater. Today Proc.* **2020**, *33*, 4751–4755. [CrossRef]
6. Papuga, S.; Djurdjevic, M.; Ciccioli, A.; Vecchio Ciprioti, S. Catalytic Pyrolysis of Plastic Waste and Molecular Symmetry Effects: A Review. *Symmetry* **2023**, *15*, 38. [CrossRef]
7. Shah, H.H.; Amin, M.; Iqbal, A.; Nadeem, I.; Kalin, M.; Soomar, A.M.; Galal, A.M. A review on gasification and pyrolysis of waste plastics. *Front. Chem.* **2023**, *10*, 960894. [CrossRef] [PubMed]
8. Palanivelrajan, A.R.; Feroskhan, M. Comparison of various catalysts in pyrolysis process: A review. *Mater. Today Proc.* **2023**, *84*, 47–56. [CrossRef]
9. Ferrini, P.; Dijkmans, J.; De Clercq, R.; Van de Vyver, S.; Dusselier, M.; Jacobs, P.A.; Sels, B.F. Lewis acid catalysis on single site Sn centers incorporated into silica hosts. *Coord. Chem. Rev.* **2017**, *343*, 220–255. [CrossRef]
10. Zakharova, M.V.; Kleitz, F.; Fontaine, F.-G. Lewis acidity quantification and catalytic activity of Ti, Zr and Al-supported mesoporous silica. *Dalton Trans.* **2017**, *46*, 3864–3876. [CrossRef] [PubMed]
11. Hao, Y.; Zhao, D.; Liu, W.; Zhang, M.; Lou, Y.; Wang, Z.; Tang, Q.; Yang, J. Uniformly Dispersed Cu Nanoparticles over Mesoporous Silica as a Highly Selective and Recyclable Ethanol Dehydrogenation Catalyst. *Catalysts* **2022**, *12*, 1049. [CrossRef]
12. Mazarío, J.; Cecilia, J.A.; Rodríguez-Castellón, E.; Domine, M.E. Highly dispersed copper oxide on silica: Towards an efficient catalyst for continuous glycerol dehydration to acetol. *Appl. Catal. A* **2023**, *652*, 119029. [CrossRef]
13. Marin, F.; Bucura, F.; Niculescu, V.-C.; Roman, A.; Botoran, O.R.; Constantinescu, M.; Spiridon, S.I.; Ionete, E.I.; Oancea, S.; Zaharioiu, A.M. Mesoporous Silica Nanocatalyst-Based Pyrolysis of a By-Product of Paper Manufacturing, Black Liquor. *Sustainability* **2024**, *16*, 3429. [CrossRef]
14. Wang, Z.; Liu, Q.; Yu, J.; Wu, T.; Wang, G. Surface structure and catalytic behavior of silica-supported copper catalysts prepared by impregnation and sol–gel methods. *Appl. Catal. A* **2003**, *239*, 87–94. [CrossRef]
15. Dong, X.; Ma, X.; Xu, H.; Ge, Q. Comparative study of silica-supported copper catalysts prepared by different methods: Formation and transition of copper phyllosilicate. *Catal. Sci. Technol.* **2016**, *6*, 4151–4158. [CrossRef]

16. Xu, C.; Chen, G.; Zhao, Y.; Liu, P.; Duan, X.; Gu, L.; Fu, G.; Yuan, Y.; Zheng, N. Interfacing with silica boosts the catalysis of copper. *Nat. Commun.* **2018**, *9*, 3367. [CrossRef] [PubMed]
17. Wu, X.; Turnell-Ritson, R.C.; Han, P.; Schmidt, J.-C.; Piveteau, L.; Yan, N.; Dyson, P.J. Carbamate-bond breaking on bulk oxides realizes highly efficient polyurethane depolymerization. *Nat. Commun.* **2025**, *16*, 4322. [CrossRef] [PubMed]
18. Diao, S.; Qian, W.; Luo, G.; Wei, F.; Wang, Y. Gaseous catalytic hydrogenation of nitrobenzene to aniline in a two-stage fluidized bed reactor. *Appl. Catal. A* **2005**, *286*, 30–35. [CrossRef]
19. Li, X.; Zhu, R.; Sun, B.; Chen, L.; Yang, H.; Liu, X.; Guo, Y.; Wang, Y. Cu@SiO2 catalyst with high copper dispersion for chemoselective hydrogenation of p-chloronitrobenzene. *Chem. Eng. J.* **2024**, *487*, 150652. [CrossRef]
20. Sun, B.; Zou, J.; Qiu, W.; Tian, S.; Wang, M.; Tang, H.; Wang, B.; Luan, S.; Tang, X.; Wang, M.; et al. Chemical transformation of polyurethane into valuable polymers. *Natl. Sci. Rev.* **2025**, *12*, nwae393. [CrossRef] [PubMed]
21. Mara, A.; Wijaya, K.; Trisunaryanti, W. Effect of Sulfuric Acid Treatment and Calcination on Natural Zeolites of Indonesia. *Asian J. Chem.* **2016**, *28*, 11–14. [CrossRef]
22. Chaichana, E.; Boonsinvarothai, N.; Juntadech, N.; Jongsomjit, B. Catalytic dehydration of ethanol to ethylene and diethyl ether over alumina catalysts containing different phases with boron modification. *J. Porous Mater.* **2019**, *26*, 599–610. [CrossRef]
23. Smith, R.C.; Reza, M.T. Evaluation of Integral and Differential Coats–Redfern Methods for Pine Pyrolysis Kinetics. *Fire* **2026**, *9*, 101. [CrossRef]
24. *ISO 16948:2015*; Solid Biofuels—Determination of Total Content of Carbon, Hydrogen and Nitrogen. International Organization for Standardization (ISO): Geneva, Switzerland, 2015.
25. Zhuravlev, L.T. The surface chemistry of amorphous silica. Zhuravlev model. *Colloids Surf. A* **2000**, *173*, 1–38. [CrossRef]
26. Zhao, W.; Shen, M.; Zhu, Y.; Ren, X.; Li, X. Insights into Synergy of Copper and Acid Sites for Selective Catalytic Reduction of NO with Ammonia over Zeolite Catalysts. *Catalysts* **2023**, *13*, 301. [CrossRef]
27. Magiera, A.; Kuźnia, M.; Stanik, R.; Kaczorek-Chrobak, K.; Gude, M.; Papis, B.K. Flammability and Thermal Properties of Rigid Polyurethane Foams Modified with Waste Biomass and Ash. *Materials* **2025**, *18*, 4570. [CrossRef] [PubMed]
28. Rakhman, A.; Diharjo, K.; Raharjo, W.W.; Suryanti, V.; Kaleg, S. Improvement of Fire Resistance and Mechanical Properties of Glass Fiber Reinforced Plastic (GFRP) Composite Prepared from Combination of Active Nano Filler of Modified Pumice and Commercial Active Fillers. *Polymers* **2022**, *15*, 51. [CrossRef] [PubMed]
29. Mumtaz, N.; Li, Y.; Artiaga, R.; Guo, Q.; Mumtaz, A. Effects of Mg(OH)2 and MWCNTs on the thermal degradation kinetics of LLDPE in nitrogen: Part B—Non-isothermal tests. *J. Therm. Anal. Calorim.* **2025**, *150*, 11925–11945. [CrossRef]
30. Xiao, X.; Jiang, B.; Li, J.; Amirkhanian, S.N.; Xiao, F. Pyrolysis optimization for sustainable down-cycling flexible polyurethane foam in asphalt industry. *Resour. Conserv. Recycl.* **2024**, *206*, 107608. [CrossRef]
31. Wu, W.; Huang, X.; Mo, Y.; Ye, M.; Hu, Q.; Chen, Q.; Wang, Y.; Hu, C. Preparation and Flame-Retardant Properties of DMMP/Nano-Silica/WPU Composite Materials. *Polymers* **2025**, *17*, 1052. [CrossRef] [PubMed]
32. Hiltz, J.A. Analytical pyrolysis gas chromatography/mass spectrometry (py-GC/MS) of poly(ether urethane)s, poly(ether urea)s and poly(ether urethane-urea)s. *J. Anal. Appl. Pyrolysis* **2015**, *113*, 248–258. [CrossRef]
33. Levchik, S.V.; Weil, E.D. Thermal decomposition, combustion and fire-retardancy of polyurethanes—a review of the recent literature. *Polym. Int.* **2004**, *53*, 1585–1610. [CrossRef]
34. Hong, J.; Wu, T.; Wang, X.; Lu, Z.; Zhang, J.; Zeng, B.; Yuan, C.; Dai, L. Copper-catalyzed pyrolysis of halloysites@polyphosphazene for efficient carbonization and smoke suppression. *Compos. Part B* **2021**, *230*, 109547. [CrossRef]
35. Wang, X.; Li, C.; Yang, J.; Liu, Y.; Hei, J.; Huang, S.; Gao, D. Production of aromatic hydrocarbons from catalytic fast pyrolysis of microalgae over Fe-modified HZSM-5 catalysts. *RSC Adv.* **2024**, *14*, 36970–36979. [CrossRef] [PubMed]
36. Zakharyan, E.; Maksimov, A. Pyrolysis of Polyurethanes. Process Features and Composition of Reaction Products. *Russ. J. Appl. Chem.* **2022**, *95*, 191–255. [CrossRef]
37. Hosaka, S.; Kurniawan, E.; Yamada, Y.; Sato, S. Vapor-phase dehydrogenation of 1-decanol to decanal over Cu/SiO2 catalyst prepared by organic additives-assisted impregnation. *Appl. Catal. A* **2023**, *653*, 119079. [CrossRef]
38. Zhong, X.; Li, B.; Li, C.; Zhang, L.; Zhang, S.; Hu, X. Removal of the local fence-like SiO2 in rice husk facilitates pore development in activation. *Fuel* **2025**, *388*, 134466. [CrossRef]
39. Guo, X.; Zhang, W.; Wang, L.; Hao, J. Comparative study of nitrogen migration among the products from catalytic pyrolysis and gasification of waste rigid polyurethane foam. *J. Anal. Appl. Pyrolysis* **2016**, *120*, 144–153. [CrossRef]

Disclaimer/Publisher's Note: The statements, opinions and data contained in all publications are solely those of the individual author(s) and contributor(s) and not of MDPI and/or the editor(s). MDPI and/or the editor(s) disclaim responsibility for any injury to people or property resulting from any ideas, methods, instructions or products referred to in the content.